GEOPHYSICAL RESEARCH LETTERS, VOL. 27, NO. 24, PAGES 4053-4056, DECEMBER 15, 2000

Parallel electric fields in discrete arcs

R. E. Ergun

Laboratory for Atmospheric and Space Physics and the Department of Astrophysical and Planetary Sciences, University of Colorado, Boulder, CO

C. W. Carlson, J. P. McFadden, F. S. Mozer

Space Sciences Laboratory, University of California, Berkeley, CA

R. J. Strangeway

Institute for Geophysical and Planetary Physics, University of California, Los Angeles, CA

Abstract. We present a large-scale model of the parallel electric fields in the upward current region of the aurora. The model, called the "Transition Layer Model", applies to intense, discrete arcs. It is based on 1-D spatial, 2-D velocity static Vlasov simulations and observations from the Fast Auroral Snapshot (FAST) satellite. The model depicts three regions along the magnetic field that are separated by two transition layers which contain parallel electric fields. The current-voltage properties closely follow the Knight relation.

Introduction

Parallel electric fields are known to be the primary acceleration mechanism in the upward current region of the aurora. They have been inferred from observations on sounding rockets and satellites [*Evans*, 1974, *Mozer et al.*, 1977] and direct measurements have been reported [*Mozer and Kletzing*, 1998]. Although it has been established that a parallel electric field can drive a current against the magnetic mirror force [*Knight*, 1973], a theoretical understanding of how they are supported self-consistently in a collisionless plasma or how they are distributed has not been established [see *Borovsky*, 1993 and references therein].

This article concentrates on the distribution of the parallel electric fields along the auroral field lines following several earlier studies which found quasi-neutral solutions [*Chiu and Schultz*, 1978; *Stern*, 1981]. We improve these earlier works by incorporating FAST observations, which give more realistic boundary conditions, into an advanced numerical code.

The S3-3 satellite mission established that auroral acceleration is a near-Earth process, often less than 8000 km in altitude. Subsequent missions verified this finding. The results from the Dynamics Explorer (DE) mission suggested that there were possibly two acceleration layers [*Reiff et al.*, 1988 and references therein; *Gurgiolo and Burch*, 1988]. FAST observations also suggest both high- and low-altitude acceleration regions [*Carlson et al.*, 1998]. Recent Polar observations now conclude that the majority of auroral acceleration is below 2 R_E in altitude [*Mozer and Hull*, 2000].

The large-scale solutions that we present here suggest that the parallel electric fields concentrate in two transition layers. The lower-altitude layer, called the "electron transition layer", separates the auroral cavity from the ionosphere. The auroral cavity is dominated by an ion beam of ionospheric origin and precipitating electrons of magnetospheric origin. The higher-altitude layer, called the "ion transition layer", separates the auroral cavity from the plasma sheet-dominated magnetosphere. The basic model is supported by FAST, Polar, DE observations.

Paper number 2000GL003819.
0094-8276/00/2000GL003819$05.00

II. Observations

We begin with FAST observations from the upward current region of the aurora. Similar observations and instrument descriptions have been reported [*Carlson et al.*, 1998; *Ergun et al.*, 1998a], so our presentation is brief. Figure 1 displays a 22-s (~110 km traveling northward) high-resolution snapshot of the near-midnight region of the northern aurora. The top panel, (a), plots the electric

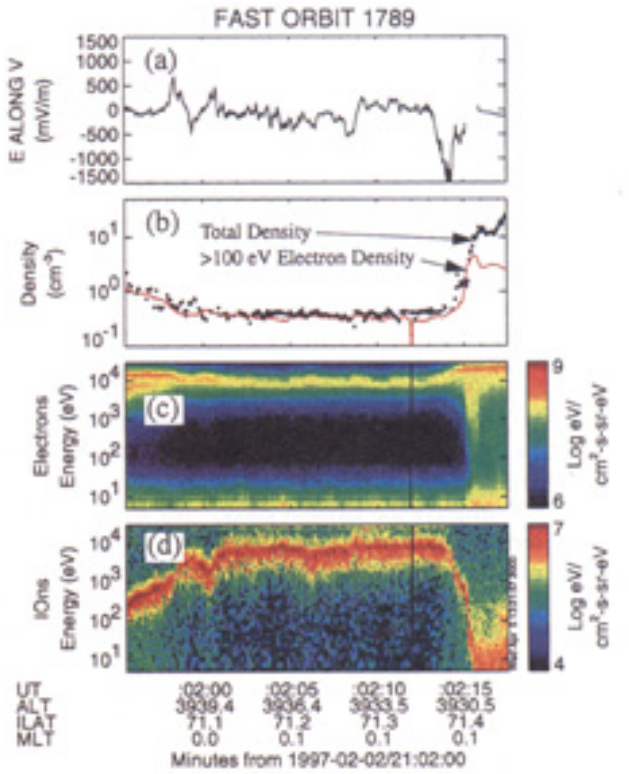

Figure 1. FAST observations of the auroral cavity. (a) The electric field perpendicular to ***B*** and nearly along the spacecraft velocity. (b) The plasma density measured by two techniques. The red trace is the density of > 100 eV electrons as measured by electrostatic analyzers. The black circles are the total plasma density as derived from the O-mode cut off. (c-d) The electron and ion energy flux versus energy and time.

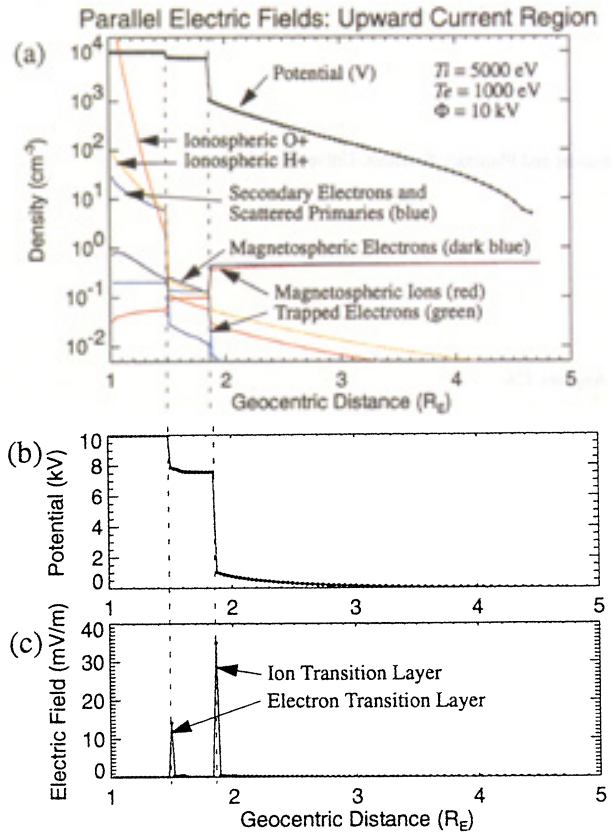

Figure 2. The results of a 1-D spatial, 2-D velocity large-scale Vlasov simulation. (a) Ionospheric O^+ (orange), ionospheric H^+ (yellow), electron secondaries and scattered primaries (blue), and cold electron distributions are specified at the left boundary. The plasma sheet electrons (dark blue) and ions (red) are specified at the left boundary. The trapped regions are filled in with the same phase space density as the magnetospheric electrons as a function of energy, up to a value of $\alpha * f_{max}$, where α =0.02. The circles represent the potential (Φ). (b) Φ on a linear scale. (c) The one pixel averaged electric field on a linear scale.

field component perpendicular to the ambient magnetic field (***B***) and nearly along the spacecraft velocity vector. The large positive excursions (~21:02:00 UT) followed by a large negative excursion (~21:02:14 UT) are indicative of a converging electric field structure which implies a parallel electric field.

Panel (c) displays the electron energy flux as a function of energy (vertical axis). Panel (d) displays the ion energy flux in the same format. From the left hand side of the plot until ~21:02:15 UT, there are downward accelerated electrons and an up-going ion beam. We conclude that there is a parallel electric field both above and below the spacecraft.

Panel (b) displays the plasma density using two different techniques. The red trace is the density derived from the electron distributions using >100 eV particles; the circles are the density derived from wave dispersion. The agreement of the quantities implies that the plasma sheet electrons dominate the auroral cavity and, notably, that there is little or no cold electron population [*Strangeway et al.*, 1998; *Ergun et al.*, 1998b; *McFadden et al.*, 1999].

After ~21:02:14 UT, the spacecraft was below the auroral cavity and therefore in a region dominated by ionospheric plasma. The electron fluxes below ~5 keV dramatically increase. The hot (>100 eV) electron density increases, but not as dramatically as the total density inferred from the wave dispersion implying a substantial cold (< 100 eV) electron population.

Table 1. Boundary Conditions

Species	Density	Temperature	Type of Distribution	Boundary
Ionospheric O^+	$2x10^5$ cm^{-3}	0.5 eV	Fluid	Left
Ionospheric H^+	100 cm^{-3}	0.5 eV	Fluid	Left
Secondaries (e^-)	30 cm^{-3}	~100 eV	Power Law: $f \sim v^{-5.25}$	Left
Scattered Primaries	1 cm-3	~1 keV	Fit to data.	Left
Ionospheric e^-	$2x10^5$ cm^{-3}	0.5 eV	Boltzman Fluid	Left
Magnetospheric H^+	0.5 cm^{-3}	5 keV	Maxwellian	Right
Magnetospheric e^-	0.5 cm^{-3}	1 keV	Maxwellian	Right
Trapped e^-	$\alpha = 0.02$		Filled Maxwellian	

III. Numerical Simulations

A static, 1-D spatial, 2-D velocity, Vlasov code was used to search for large-scale, self-constant solutions of the parallel electric

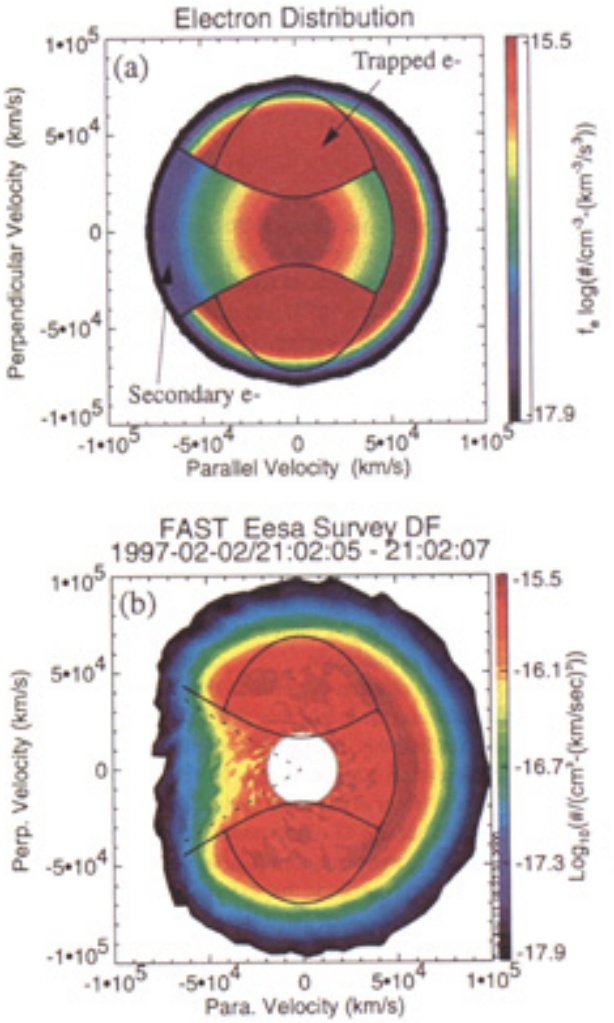

Figure 3. (a) The electron distribution from the adiabatic simulation. The boundaries between the magnetospheric, secondary and scattered primary, and trapped electrons are marked with solid lines. (b) An electron distribution in the auroral cavity in Figure 1 as measured by FAST. The dashed lines are the loss cone with no electric field. The distributions are quantitatively similar except in the region of secondary and scattered primary electrons. Velocity space diffusion may account for the differences between the distributions.

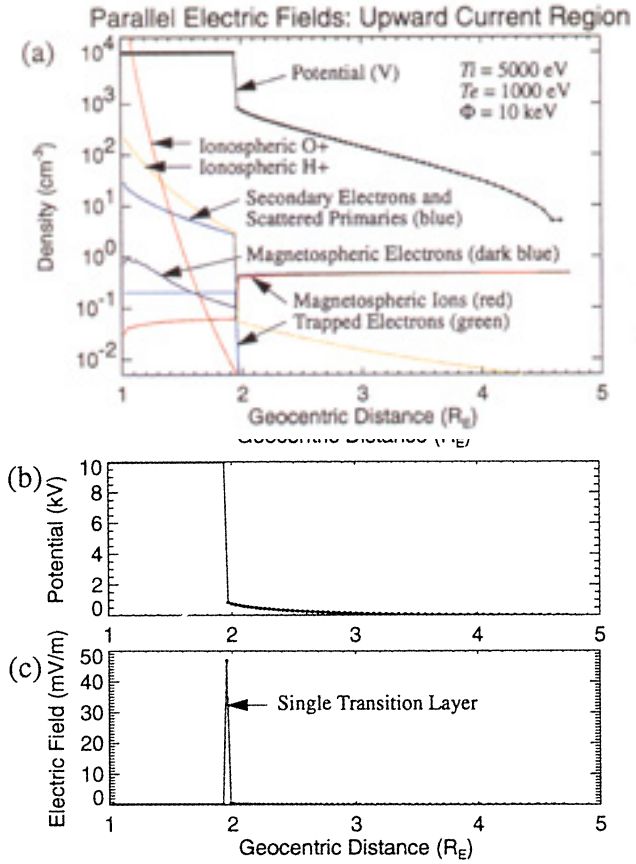

Figure 4. The simulation in Figure 2 repeated with 1/2 of the ionospheric H^+ density and the trapped electrons reduced by 25%.

Figure 2 displays the results of the simulation. The horizontal axis represents geocentric distance in Earth-radii and the vertical axis represents density or potential. The left hand side is the ionospheric boundary at which cold O^+, cold H^+, cold electrons, electron secondaries, and scattered primaries are prescribed (Table 1). The cold ion populations are treated as fluids and the cold electron population is treated as a Boltzman fluid ($n \propto e^{e\Phi/T_e}$); it conforms to the ion density via an ambipolar electric field. The right hand side of Figure 2 is the magnetospheric boundary which has prescribed plasma sheet ion (5 keV H^+) and electron distributions (1 keV) that are consistent with the observations in Figure 1.

One can see three distinct regions separated by two transition layers. The low-altitude aurora is dominated by ionospheric plasma. The cold O^+ and H^+ populations fall rapidly due to gravitational attraction. The auroral cavity is filled with an ion beam of ionospheric origin and plasma sheet electrons and the high-altitude aurora is controlled by plasma sheet electrons and ions. The simulation results are consistent with FAST, Polar, and DE results.

Figure 3 compares the measured electron distributions in the auroral cavity with those in the simulation on the identical scales. The boundaries between the accelerated, trapped, and secondary/scattered primary electrons are marked on the simulation. The same boundaries, scaled to accommodate slightly lower energies (96%), are marked on the FAST distributions. The distributions are quantitatively similar. The main difference is in the phase space density of the secondary electron region. The FAST data indicates velocity space diffusion may increase the phase space density. This region, fortunately, does not contribute substantially to the overall density.

In all of the simulations, the thickness of the low-altitude, or electron transition layer, is the grid size ($\Delta z \sim 250$ km). Simulations

field. A description of similar, non-static Vlasov codes can be found in *Cheng and Knorr* [1976]; the static simulations do not use regridding. The basic idea is as follows. Electron and ion distributions are prescribed at the boundaries of a large spatial region which has a mirroring magnetic field. The potential at the boundaries are also prescribed and the region is initiated with an estimated potential distribution, $\Phi(z)$. The distributions are broken into N_v x N_v velocity-space elements (N_v = 70 or 50 in the simulations we present), each of which is treated as a fluid. Trapped electrons, an important part of the distribution (see later), are filled in with the same phase space density as the magnetospheric electrons as a function of energy, up to a value of $\alpha * f_{max}$. The parameter α (~0.02) is adjusted to best match the FAST distributions. f_{max} is the maximum phase space density of the magnetospheric electrons. Using the prescribed distributions at the boundaries and $\Phi(z)$, the velocity space distributions are calculated at N_z (= 99) spatial locations between the boundaries. An error is defined as:

$$\xi(z) = \nabla^2\Phi + \frac{e}{\varepsilon_o}(n_i - n_e) \qquad (1)$$

where n_i and n_e are the ion and electron densities derived from the distributions. $\Phi(z)$ is then iteratively adjusted to minimize $\xi(z)$ which yields a static solution. In the simulations here, the grid spacing ($\Delta z \sim 250$ km in the displayed simulations) is much larger than the Debye length ($\lambda_D \sim 1$ km) so the $\nabla^2\Phi$ term is negligible, which essentially results in an quasi-neutral solution. The static code enforces adiabatic evolution (no velocity-space diffusion) and therefore yields in the Knight current-voltage relation. Gravitational potential is included.

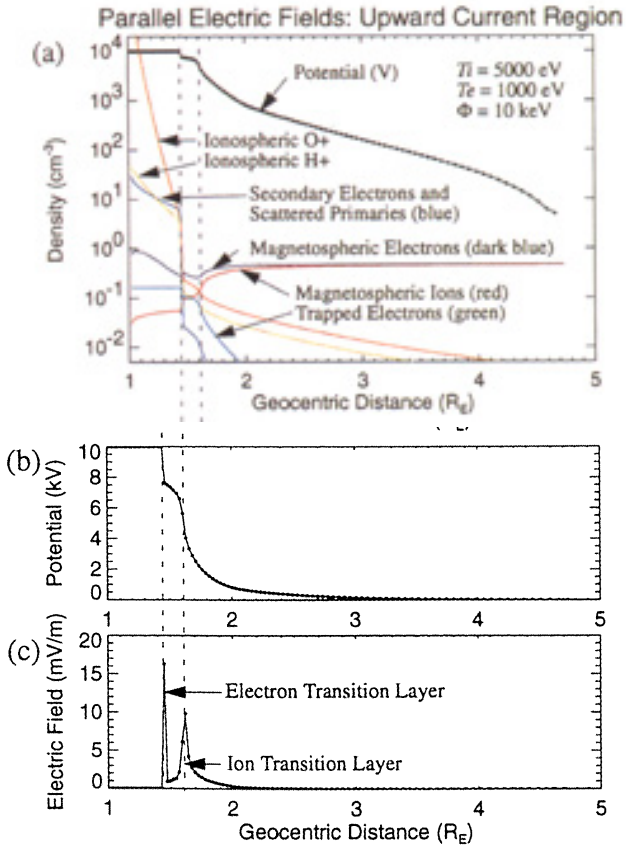

Figure 5. The simulation in Figure 2 repeated with 2.5 times ionospheric H^+ density.

with Δz as small as ~125 km have the same result. The electron transition layer forms at the altitude at which the density of electron secondaries and scattered primaries equals the cold ion density. The ionospheric density altitude profile plays a strong role. If the H^+ density is lower, the altitude of the electron transition layer is lower, and the ion beam is O^+ dominated (Figure 3). If the H^+ density is increased, the electron transition layer appears at a higher altitude. In the extreme case, if the ion density altitude profile is such that the above condition is not met, the electron transition layer does not appear (Figure 4). These results are in consort with the seasonal variations of the altitude of the auroral cavity [*Temerin et al.*, 1998].

The high-altitude parallel electric field, or ion transition layer, is located near ~1 R_E in altitude. The potential above the ion transition layer has a monotonic ramp, increasing with decreasing altitude. The abrupt jump in potential, once again, is one grid point in Figure 2. We find that, if the potential jump ($\Delta\Phi_i$) is lower than the plasma sheet ion temperature, T_{psi}, the abrupt (one grid size) potential jump is no longer seen (Figure 5). It is replaced with a peaked electric field structure spread over a distance of O(0.1) R_E. The trapped electron density was decreased for the example in Figure 5 to α = 0.015 to cause $\Delta\Phi_i < T_{psi}$; lowering the total potential drop has the same effect. The spread parallel electric field result is favored by the Polar observations [*Mozer and Hull*, 2000]

The region between the transition layers, which we define as the auroral cavity, has a low-level parallel electric field. The electric field maintains a quasi-neutral environment between two species whose densities evolve in altitude differently.

IV. Discussion and Conclusions

We have presented a large-scale representation of the parallel electric fields based on 1-D spatial, 2-D velocity static Vlasov simulations. It is applicable to discrete arcs with large acceleration potentials (> 5 keV). The model is strongly supported by FAST, Polar and DE observations. The simulations predict:

(1) Three distinct regions separated by two transition layers. The low-altitude region is dominated by ionospheric plasma, the high-altitude region by plasma sheet populations. The region in between, the auroral cavity, is dominated by ionospheric ions and magnetospheric electrons.

(2) A low-altitude, or electron transition layer, when present, is seen at one grid space in all simulations. It is less than 128 km thick.

(3) The electron transition layer appears at the altitude at which the density of the electron secondaries and scattered primaries equals the cold ion density. If the above condition is not met, no transition layer appears. When present, it is between ~2000 km and ~5000 km in altitude and depends on the altitude profile of the ion density. Lower ion density (or stronger precipitating electron energy flux and hence higher electron secondary density) causes the layer to appear at lower altitude.

(4) The high-altitude, or ion transition layer is seen near 1 R_E in altitude under the conditions in the simulation.The altitude at which it appears depends on the magnetospheric plasma and the current density (or total potential drop). With higher current density the ion transition layer moves to higher altitude.

(5) The ion transition layer is less than 128 km (the minimum Δz) if the potential jump across the layer exceeds ~T_{psi}. Otherwise, a broad-scale, peaked electric field structure is seen.

We must caution that (1) the simulations results may not be unique, (2) the trapped electron population was imposed by an empirical formula, (3) velocity-space diffusion has not been accounted for, and (4) the resulting potential structures may not be stable. The large-scale results, however, provide a basis to investigate the time-dependent, self-consistent parallel electric fields and are suggestive of the parallel electric field concentrating in large double layers [*Block*, 1972] in intense arcs.

Acknowledgments. The authors thank D. Newman for helpful discussions. This research was conducted under NASA grants NAG5-3596 and NAG-9353.

References

Block, L. P., Potential double layers in the ionosphere, *Cosmic Electrodyn.*, 3, 349, 1972.

Borovsky, Joseph E., Auroral arc thicknesses as predicted by various theories, *J. Geophys. Res.*, 98, 6101, 1993.

Carlson, C. W., R. F. Pfaff, and J. G. Watzin, The Fast Auroral Snapshot (FAST) mission, *Geophys. Res. Lett.*, 25, 2013, 1998.

Cheng, C. Z., and G. Knorr, The integration of the Vlasov equation in configuration space, *J. Comput. Phys.*, 22, 330-351, 1976.

Chiu, Y. T., and M. Schultz, Self-consistent particle and parallel electrostatic field distributions in the magnetospheric-ionospheric auroral region, *J. Geophys. Res.*, 83, 629, 1978.

Ergun, R. E. et al., FAST satellite observations of electric field structures in the auroral zone, *Geophys. Res. Lett.*, **25,** 2025, 1998a.

Ergun, R. E. et al., FAST satellite wave observations in the AKR source region, *Geophys. Res. Lett.*, **25,** 2061, 1998b.

Evans, D. S., Precipitation electron fluxes formed by a magnetic-field-aligned potential difference, *J. Geophys. Res.*, 79, 2853, 1974.

Gurgiolo, C. and J. L. Burch, Simulation of electron distributions within auroral acceleration regions, *J. Geophys. Res.*, 93, 3989, 1988.

Knight, S., Parallel electric fields, *Planet. Space Sci.*, 21, 741, 1973.

McFadden, J. P., C. W. Carlson, R. E. Ergun, D. M. Klumpar, and E. Moebius, Ion and electron characteristics in auroral density cavities associated with ion beams: No evidence for cold ionospheric plasma, *J. Geophys. Res.*, 104, 14671, 1999.

Mozer, F. S., C. W. Carlson, M. K. Hudson, R. B. Torbert, B. Parady, J. Yatteau, and M. C. Kelley, Observations of paired electrostatic shocks in the polar magnetosphere, *Phys. Rev. Lett.*, 38, 292, 1977.

Mozer, F. S., and C. A. Kletzing, Direct observation of large, quasi-static, parallel electric fields in the auroral acceleration region, *Geophys. Res. Lett.*, **25**, 1629, 1998.

Mozer, F. S., and A. Hull, The origin and geometry of upward parallel electric fields in the auroral acceleration region, *J. Geophys. Res.*, submitted, 2000.

Reiff, P. H., H. L. Collin, J. D. Craven, J. L. Burch, and J. D. Winningham, Determination of auroral electrostatic potentials using high- and low-altitude particle distributions, *J. Geophys. Res.*, 93, 7441, 1988.

Stern, D. P., One-dimensional models of quasi-neutral parallel electric fields, *J. Geophys. Res.*, 86, 5839, 1981.

Strangeway, R. J. et al., FAST observations of VLF waves in the auroral zone: Evidence of very low plasma densities, *Geophys. Res. Lett.*, **25,** 2065, 1998.

Temerin, M. and C. W. Carlson, Asymmetry of occurrence-frequency and intensity of AKR between summer polar region and winter polar region sources, *Geophys. Res. Lett.*, 25, 2369, 1998.

C. W. Carlson, J. P. McFadden, F. S. Mozer, Space Sciences Laboratory, University of California, Berkeley, CA 94720. (e-mail: cwc@ssl.berkeley.edu; mcfadden@ssl.berkeley.edu; mozer@ssl.berkeley.edu)

R. E. Ergun, Laboratory for Atmospheric and Space Physics, University of Colorado, Boulder, CO 80303. (e-mail: ree@fast.colorado.edu)

R. Strangeway, IGPP, University of California, Los Angeles, CA 90095. (e-mail: strange@igpp.ucla.edu)

(Received May 18, 2000; revised September 11, 2000;
accepted September 20, 2000.)